Simultaneous inversion of velocity and angle-dependent reflectivity

Nizar Chemingui, Yang Yang, Jaime Ramos-Martinez, Guanghui Huang, Dan Whitmore, Sean Crawley, Elena Klochikhina, and Sriram Arasanipalai, PGS*

Summary

We introduce an innovative technique for simultaneous inversion of velocity and angle-dependent reflectivity. The key aspect of our method lies in extracting angle information from the solution of the vector-reflectivity-based wave equation, which is a crucial step in the process. The incorporation of pre-stack angle gathers significantly enhances our understanding of subsurface and reservoir properties. The outcomes of our approach encompass the velocity model, reflectivity image, and pre-stack angle gathers, along with the derived relative density and impedance. These results provide valuable insights for conducting reliable amplitude versus angle (AVA) analysis and quantitative interpretation (QI).

Introduction

Seismic attributes play a crucial role in hydrocarbon exploration by identifying potential prospects. To obtain earth models for velocity and reflectivity, seismic inversion has been the traditional approach, followed by attribute calculations aiding interpretation.

We have developed an innovative simultaneous inversion workflow utilizing a vector reflectivity parameterization of the wave equation (Whitmore et al., 2021) and an efficient scale separation of the FWI gradient through inverse scattering theory (Whitmore and Crawley, 2012; Ramos-Martinez et al., 2016). This approach enables iterative estimation of both velocity and earth reflectivity within a single framework (Yang et al., 2022), allowing us to derive relative impedance and density for prospectivity assessment.

Seismic amplitude variations with angle can provide valuable insights into fluid content, porosity, and lithology of subsurface formations for a deeper understanding of subsurface geology. However, conventional solutions for Full Waveform Inversion (FWI) do not straightforwardly compute pre-stack reflectivity, which is crucial for AVA analysis.

In our work, we expand on Yang et al.'s (2022) simultaneous inversion workflow, which updates velocity and stacked 3D reflectivity, by incorporating angle and azimuth-dependent pre-stack reflectivity. Our method employs geometric information extracted from the dot product between the vector reflectivity and the gradient of the pressure wavefield in the relevant wave equation. This enables us to compute the angle between the incident wavefield and the vector reflectivity, thereby facilitating the construction of angle gathers. Through our simultaneous inversion process, we continually update the velocity model and angle gathers, leading to improved model resolution and compensating for incomplete acquisitions and variations in illumination.

Method

We begin with the acoustic wave equation, represented in terms of velocity and vector reflectivity (Whitmore et al., 2021):

$$\frac{1}{V(\boldsymbol{x})^2}\frac{\partial^2 P(\boldsymbol{x},t)}{\partial t^2} - \nabla^2 P(\boldsymbol{x},t) - \frac{\nabla V(\boldsymbol{x})}{V(\boldsymbol{x})}\cdot\nabla P(\boldsymbol{x},t) + 2\boldsymbol{R}(\boldsymbol{x})\cdot\nabla P(\boldsymbol{x},t) = S(\boldsymbol{x},t)$$

In this equation, P represents the pressure wavefield, V denotes the velocity, and R(x) is the vector reflectivity defined as,

$$\boldsymbol{R}(\boldsymbol{x}) = \frac{1}{2}\frac{\nabla Z(\boldsymbol{x})}{Z(\boldsymbol{x})}$$

where Z is the acoustic impedance, and the source term is represented by S(x,t).

With this parameterization, we directly set velocity and reflectivity as model parameters, eliminating the need to construct a density model. The sensitivity kernels for velocity and impedance obtained through inverse scattering theory (Whitmore and Crawley, 2012; Ramos-Martinez et al., 2016), are combined with the special representation of the wave equation, forming the basis for the simultaneous inversion of velocity and reflectivity (Yang et al., 2022).

To generate angle gathers, it is essential to compute the incidence and reflection angles (or reflector dip direction) at each image point. The vector reflectivity wave equation possesses a fundamental feature that allows for the calculation of these angles. Specifically, the gradient of the forward propagation wavefield provides the direction of the incident wavefield, whereas the vector reflectivity contains information about the reflector. As a result, we can naturally extract the reflection angle required for constructing pre-stack angle gathers as follows:

$$\theta = \arccos\left(\frac{\boldsymbol{R}\cdot\nabla P}{\|\boldsymbol{R}\|\cdot\|\nabla P\|}\right)$$

Figure 1 illustrates the geometric definition of these elements and their relationship with the reflection angle and its azimuth. Once this information is acquired, the generation of angle gathers follows a process similar to that used in reverse time migration where angle and azimuth maps are computed for each individual shot and used for the binning of the pre-stack images.

DOI:10.1190/image2023-3910631.1

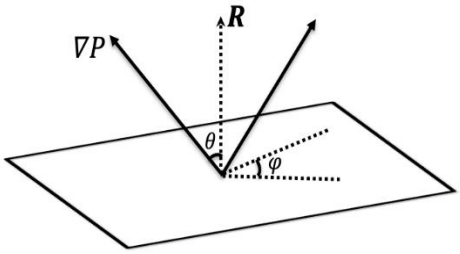

Figure 1 *Geometric relation between reflection angle, vector reflectivity and the gradient of the pressure field.*

The forward and backward propagation are based on the wave equation and its adjoint, both parameterized in terms of velocity and vector reflectivity. The modeling process incorporates the reflectivity extracted from the current angle gathers, which are updated at each iteration. The solution can also output azimuth gathers by incorporating azimuth maps, which enable further characterization of subsurface structures with azimuth information.

Examples

We discuss the effectiveness of our workflow using field data acquired in the Salar Basin located in southeast Newfoundland and Labrador, Canada. The field survey took place in 2020, utilizing multisensor streamer technology. The survey comprised 16 cables with 100-meter streamer separation and an 8-km streamer length. Previous analyses of existing seismic data have identified several fan systems along the margin, which are interpreted as Oligocene in age, with the main prospectivity believed to reside in these fans originating from the shelf and shelf edge deltas. Within the reservoir interval, Class II anomalies are observed, along with Class IV responses in the deeper section, analogous to a modeled source rock in the region. The average water column depth exceeds 3 km in this area.

The primary goal of the study was to construct a detailed higher-resolution velocity model while better defining the target fan system. The aim was to refine the velocity over the lead and provide reliable pre-stack angle-dependent reflectivity for further interpretation analysis. The successful achievement of these objectives would significantly contribute to de-risking exploration activities in this basin.

In the inversion process, we used a maximum frequency of 40 Hz and an initial velocity model that is a smoothed version of a tomographic velocity model. The simultaneous inversion significantly improved the background model and greatly enhanced the resolution (Figure 2A). The final reflectivity, equivalent to a non-linear least-squares RTM, is shown in Figure 2B. Importantly, the angle gathers (Figure 2C) were directly generated and updated at each iteration using the updated velocity and reflectivity fields, without the need for additional migrations. The improvement in the coherency of reflectors below the Cretaceous level was evident in the results, supported by the quality of the angle gathers and partial stacks, e.g., near and far angle stacks shown in Figures 2E and 2F respectively.

The inversion of velocity and reflectivity models also enabled the derivation of additional properties, including relative impedance and density (Yang et al., 2022). In Figure 3, depth slices at the target reservoir level demonstrated detailed and structurally conforming velocity updates (Figure 3C). The relative density derived from velocity and reflectivity (Figure 3D) showed a strong correlation with other earth properties. Remarkably, the prospect zone displayed a decrease in both velocity and density. Figures 3E and 3F display the reflectivity as function of angles, i.e., near vs. far-angle stacks. The results highlight clear evidence of AVO presence, providing valuable information for reservoir attribute estimation.

Conclusions

We introduced a novel extension to our simultaneous velocity and reflectivity inversion method, with the specific goal of generating angle gathers as an output. This advancement significantly enhances our understanding of subsurface properties and facilitates a more comprehensive analysis of reservoirs. Our approach leverages the wave equation, which is parameterized in terms of velocity and vector reflectivity, to extract valuable angle information about the earth properties. Through an iterative inversion workflow, we achieve simultaneous updates to both the velocity model and the angle-dependent reflectivity.

We applied our solution to a field survey from offshore Newfoundland and Labrador, Canada. The results demonstrate successful updates to the velocity model and the generation of accurate estimates of angle-dependent reflectivity. The final models include inverted velocity and reflectivity models, as well as derived relative impedance and density maps. Additionally, our new inversion process allows us to produce pre-stack angle gathers that serve as reliable inputs for subsequent analyses such as Quantitative Interpretation (QI) and Amplitude Versus Angle (AVA).

Acknowledgments

The authors would like to thank PGS for granting permission to publish this paper and providing the data used in this study through PGS multiclient. We also thank the Oil and Gas Corporation of Newfoundland and Labrador (OilCo) for their valuable support.

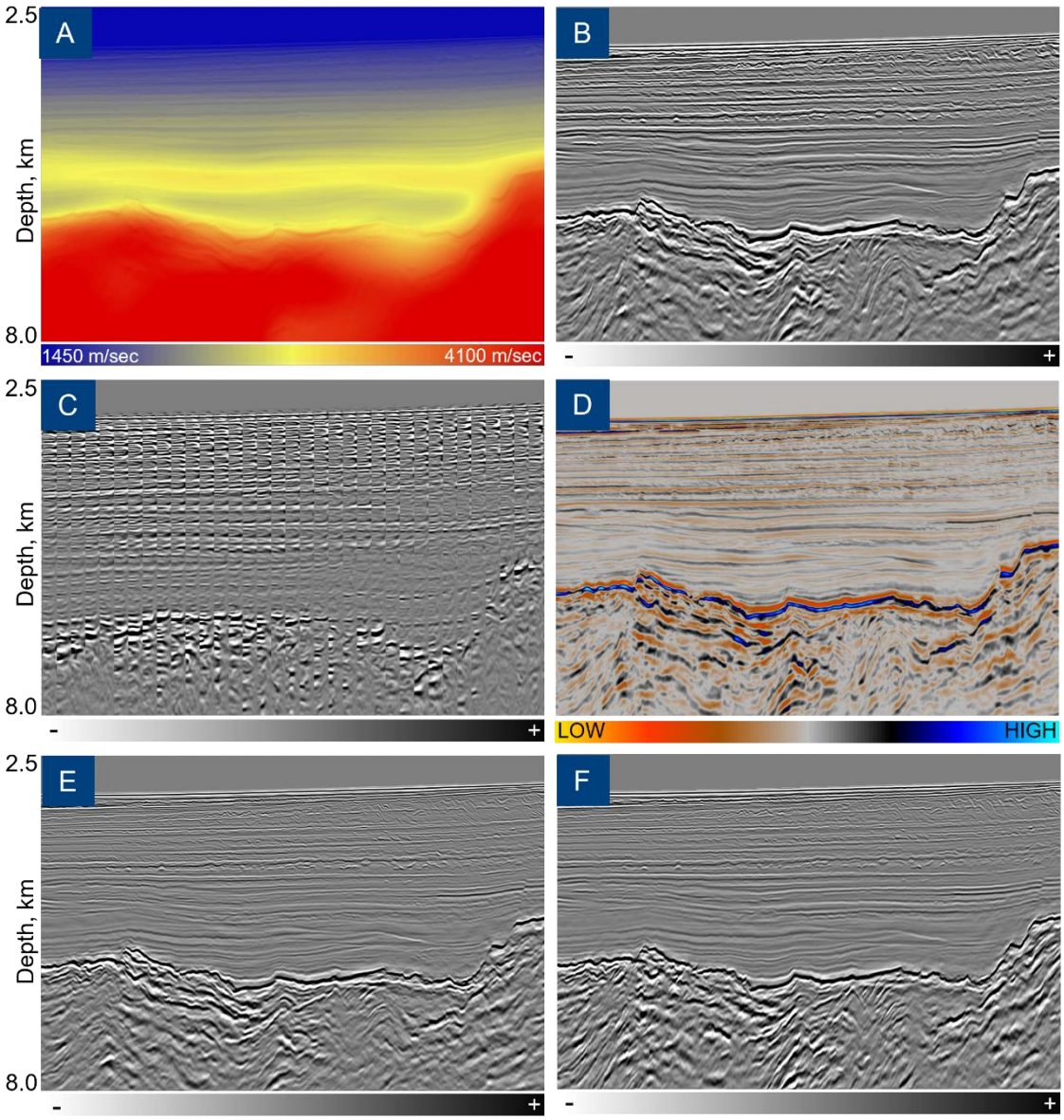

Figure 2: Inline sections of: (A) inverted velocity, (B) full-stack of reflectivity; (C) angle gathers, (D) relative density, (E) near-angle stack and (F) far-angle stack.

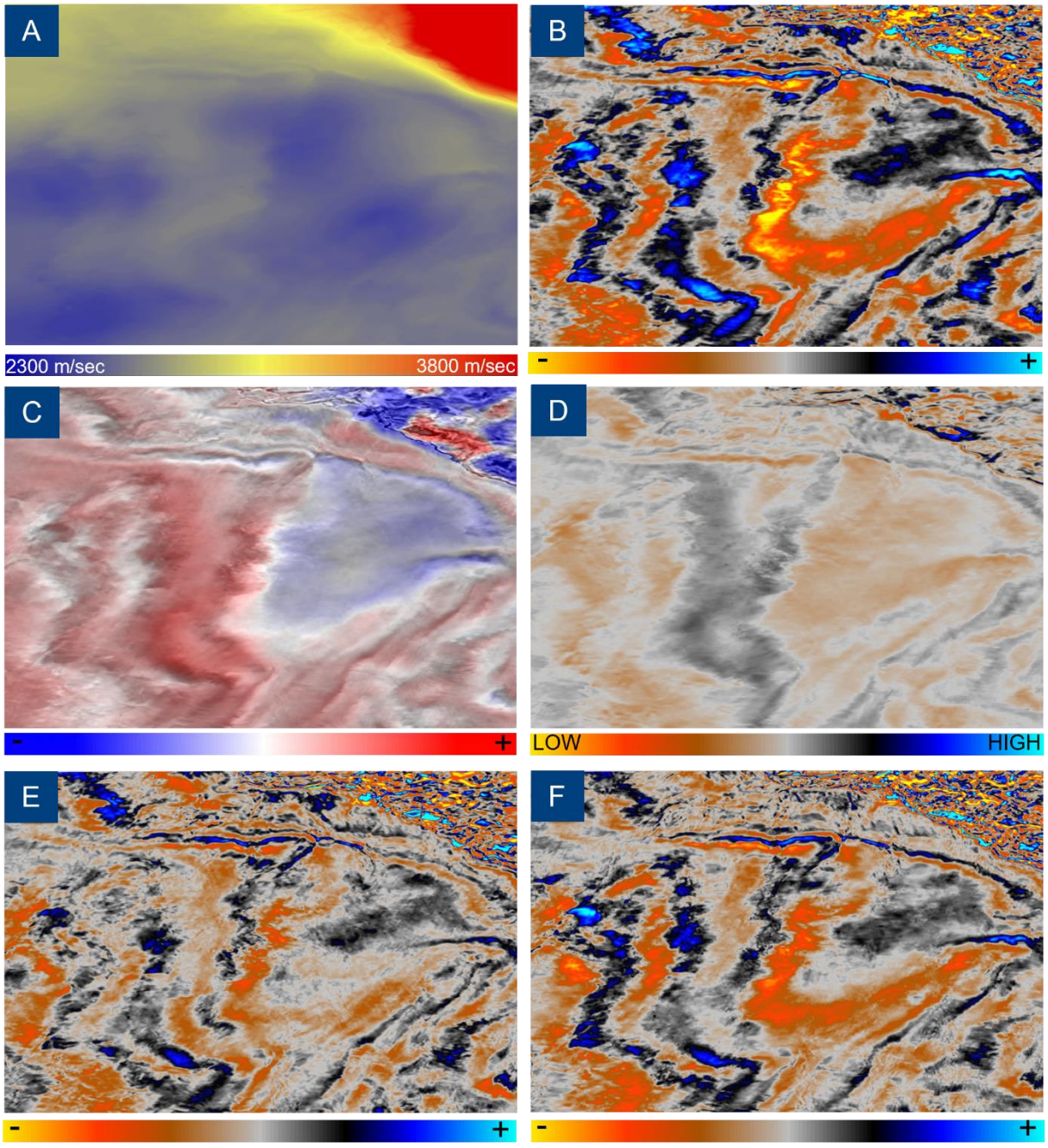

Figure 3: Depth slices extracted at reservoir level (5000m) for: (A) inverted velocity, (B) full-stack reflectivity, (C) velocity perturbation overlaying structural image, (D) relative density, (E) near-stack reflectivity, and (F) far-stack reflectivity.

REFERENCES

Ramos-Martinez, J., S. Crawley, K. Zou, A. A. Valenciano, L. Qiu, and N. Chemingui, 2016, A robust gradient for long wavelength FWI updates: 78th Annual International Conference and Exhibition, EAGE, Extended Abstracts, 1–5, doi: https://doi.org/10.1071/ASEG2016ab133.

Whitmore, N. D., and S. Crawley, 2012, Application of RTM inverse scattering imaging conditions: 82nd Annual International Meeting, SEG, Expanded Abstracts, 1–6, doi: https://doi.org/10.1190/segam2012-0779.1.

Whitmore, N. D., J. Ramos-Martinez, Y. Yang, and A. A. Valenciano, 2021, Full wavefield modeling with vector reflectivity: 83rd Annual International Conference and Exhibition, EAGE, Extended Abstracts, doi: https://doi.org/10.3997/2214-4609.202010332.

Yang, Y., N. Chemingui, S. Arasanipalai, and Ø. Korsmo, 2023, Estimating reliable earth properties from simultaneous inversion of velocity and angle-dependent reflectivity: 84th EAGE Annual Conference and Exhibition Workshop Programme, 1–5, doi: https://doi.org/10.3997/2214-4609.2023101539.

Yang, Y., J. Ramos-Martinez, N. D. Whitmore, G. Huang, and N. Chemingui, 2022, Simultaneous inversion of velocity and reflectivity: First International Meeting for Applied Geoscience & Energy, Expanded Abstracts, doi: https://doi.org/10.1190/segam2021-3594405.1.